

# RESOLVING THE UNRESOLVED COSMIC X-RAY BACKGROUND IN THE *CHANDRA* DEEP FIELDS

RYAN C. HICKOX AND MAXIM MARKEVITCH

Harvard-Smithsonian Center for Astrophysics, 60 Garden Street, Cambridge, MA 02138

*Submitted to ApJ Letters*

## ABSTRACT

We present a measurement of the surface brightness of the cosmic X-ray background (CXB) in the *Chandra* Deep Fields North and South (CDF-N and CDF-S), after excluding all detected X-ray, optical and infrared sources. The work is motivated by a recent X-ray stacking analysis by Worsley and collaborators, which showed that galaxies detected by *HST* but not by *Chandra* may account for most of the unresolved CXB at  $E > 1$  keV. We find that after excluding *HST* and *Spitzer* IRAC sources, some CXB still remains but it is barely significant:  $(3.4 \pm 1.4) \times 10^{-13}$  ergs cm<sup>-2</sup> s<sup>-1</sup> deg<sup>-2</sup> in the 1–2 keV band and  $(4 \pm 9) \times 10^{-13}$  ergs cm<sup>-2</sup> s<sup>-1</sup> deg<sup>-2</sup> in the 2–5 keV band, or  $7\% \pm 3\%$  and  $4\% \pm 9\%$ , respectively, of the total CXB. Of the 1–2 keV signal resolved by the *HST* sources,  $\simeq 66\%$  comes from objects with colors typical of starburst and irregular galaxies, while objects with “normal” galaxy colors contribute  $\simeq 34\%$ . In the 0.65–1 keV band (just above the bright Galactic O VII line and including the Fe XVII lines) the remaining intensity is  $(12 \pm 2) \times 10^{-13}$  ergs cm<sup>-2</sup> s<sup>-1</sup> deg<sup>-2</sup>. This provides a conservative upper limit on the brightness of the warm-hot intergalactic medium (WHIM) that comes interestingly close to predictions for WHIM emission. A WHIM simulation that accounts for the particular selection of the CDF pointings may constrain the WHIM metallicity.

*Subject headings:* methods: data analysis — X-rays: diffuse background — X-rays: galaxies

## 1. INTRODUCTION

The cosmic X-ray background (CXB) is known to be primarily the integrated emission from X-ray point sources, mostly active galactic nuclei (e.g., Hasinger et al. 2005; Bauer et al. 2004). Recent studies have shown that the *Chandra* Deep Fields (CDFs) North and South, the most sensitive observations of the X-ray sky to date, resolve  $\sim 80$  of the extragalactic CXB at 1–2 keV (Moretti et al. 2003; Worsley et al. 2005; Hickox & Markevitch 2006, hereafter HM06), and  $\sim 50\%$  at 7 keV (Worsley et al. 2005). While the majority of the CXB at  $E < 5$  keV has been accounted for, the nature of the still-unresolved component (the absolute intensity of which we derived in HM06) remains unclear.

Part of the unresolved CXB is almost certainly due to faint point sources that have yet to be detected in X-rays. However, HM06 showed that an extrapolation of the observed  $\log N/\log S$  curve to zero fluxes falls far short of the unresolved CXB. For this, the slope of the relation must steepen below the CDF-N X-ray source detection limit of  $S_{0.5-2 \text{ keV}} = 2.4 \times 10^{-17}$  ergs cm<sup>-2</sup> s<sup>-1</sup>. This is not implausible; Bauer et al. (2004) showed that the CDFs contain a population of normal and starburst galaxies with  $S_{0.5-2 \text{ keV}} < 10^{-16}$  ergs cm<sup>-2</sup> s<sup>-1</sup> whose  $\log N/\log S$  is indeed steeper, and which should dominate the source counts at  $S_{0.5-2 \text{ keV}} < 10^{-17}$  ergs cm<sup>-2</sup> s<sup>-1</sup>. These faint sources, while not detected in X-rays, can be associated with optical or infrared sources found in the multiwavelength observations in CDFs. A recent X-ray stacking analysis of *Hubble Space Telescope* (*HST*) sources in the CDFs has found that their X-ray emission can account for most of the unresolved  $E = 1 - 6$  keV CXB (Worsley et al. 2006).

Alternatively, some of the unresolved CXB may be truly diffuse. It may come from the warm-hot intergalactic medium (WHIM), with temperatures  $10^5$ – $10^7$  K,

that is thought to comprise the majority of the baryons outside galaxy groups and clusters in the local Universe (e.g., Cen & Ostriker 1999; Davé et al. 2001). Models of the WHIM predict a signal dominated by line emission from oxygen and iron with prominent lines at 0.5–0.8 keV, but some signal up to 1.5 keV (Phillips et al. 2001; Fang et al. 2005; Ursino & Galeazzi 2006). There have been reports of detection of X-ray absorption lines by the WHIM (e.g., Nicastro et al. 2005, however see Kaasstra et al. 2006). Diffuse emission could also come from more exotic scenarios such as decay of dark matter particles (e.g., Abazajian et al. 2007).

In this Letter we seek to constrain the diffuse CXB using an independent approach to that of Worsley et al. (2006), by directly measuring the absolute intensity of the CXB in the CDFs after the removal of all sources detected in deep X-ray, optical, and IR observations. Our analysis is a follow-up to that of HM06, in which we excluded only the X-ray sources.

## 2. DATA

*Chandra* X-ray observations of the CDFs North and South (CDF-N and CDF-S) have respective total exposure times of roughly 2 Ms and 1 Ms. The CDF-N data consists of two subsets, observed in in Very Faint (VF) or Faint (F) telemetry mode. Each of the three subsets (CDF-N VF, CDF-N F, and CDF-S) contains 6 to 9 individual observations with exposure times 30 to 170 ks each. The datasets are identical to those used in HM06, except for the ACIS calibration updates. For subtraction of the instrumental background, we add the latest ACIS stowed observations giving a total background exposure of 325 ks, compared to 256 ks used in HM06. These updates caused no significant change to the CXB fluxes.

To exclude the contributions of faint galaxies to the unresolved CXB, we use sources detected in the optical and IR observations of the Great Observatories Origins Deep

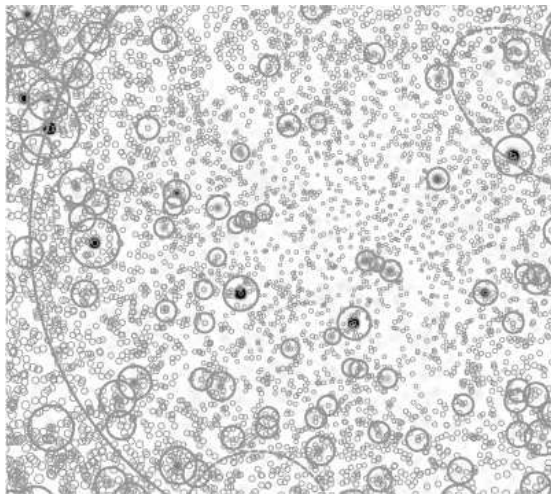


FIG. 1.— Smoothed 0.5–8 keV image of CDF-N, showing the source exclusion regions. The large circle is the 3.2' extraction region, medium-size circles and ellipses show X-ray point and extended sources, and small circles show *HST* sources.

Survey (GOODS, Dickinson et al. 2003). Optical and near-IR data were taken using the Advanced Camera for Surveys (ACS) on *HST* in the  $B_{435}$ ,  $V_{606}$ ,  $i_{775}$ , and  $z_{850}$  bands (Giavalisco et al. 2004). We use the public catalog<sup>1</sup> based on detections in the  $z_{850}$  band (which samples wavelengths  $\sim 8300$ – $9500$  Å), with a limiting magnitude of  $z_{850} \simeq 27$ . Within the regions for which we extract CXB spectra (§ 3), the *HST* catalogs for CDF-N and CDF-S each contain  $\sim 4500$  objects.

We also exclude sources detected with the Infrared Array Camera (IRAC) on *Spitzer*, in four bands centered on 3.6, 4.5, 5.8, and 8  $\mu\text{m}$ . There is no published catalog currently available for these sources, so we have performed our own source detection using the calibrated IRAC images<sup>2</sup>. Sources were detected using the **SExtractor** code (Bertin & Arnouts 1996) in all four bands. In the most sensitive band (3.6  $\mu\text{m}$ ), we detect  $\sim 1000$  sources in each spectral extraction region to a  $5\sigma$  limiting flux of  $\sim 0.2$   $\mu\text{Jy}$ . Most ( $>95\%$ ) of the IRAC sources have counterparts within  $1''$  in the *HST*  $z_{850}$  catalog.

We also considered *Spitzer* Multiband Imaging Photometer (MIPS) 24  $\mu\text{m}$  sources<sup>3</sup> and for CDF-N, Very Large Array (VLA) 21 cm sources (Richards 2000), with limiting fluxes of 80 and 40  $\mu\text{Jy}$ , respectively. All the sources within our spectral extraction regions have *HST* or IRAC counterparts, except for 2–4 of the 80–90 MIPS sources, and 1 of the 6 VLA sources, so we do not include these data in the analysis.

### 3. ANALYSIS

We calculate the CXB surface brightness as discussed in detail in § 5 of HM06, with only minor differences. For the *HST* and IRAC sources not detected in X-rays, we use smaller exclusion regions with radii equal to the 90% X-ray flux inclusion radius  $r_{90}$  (see Eqn. 1 of HM06), compared to  $4.5$ – $9r_{90}$  for X-ray sources. Due to the large number of optical and IR sources, at off-axis angles  $\theta > 3.2'$  (where  $r_{90} > 2.2''$ ) there is little area remaining

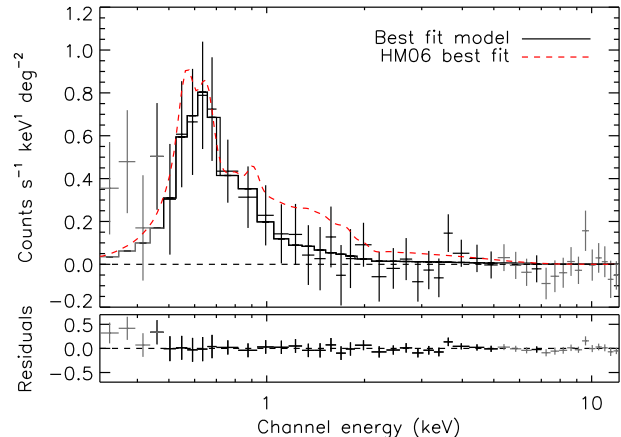


FIG. 2.— CXB spectrum for the CDF-N VF subset, with all sources (*Chandra*, *HST* and IRAC) excluded. The spectrum is fit with an APEC model with  $kT = 0.20$  keV plus a power law with  $\Gamma = 1.5$ . Black points show the data included in the fit (see HM06), and the red dashed line shows the best-fit model for the CDF-N VF spectrum excluding only X-ray sources (HM06).

after source exclusion. Therefore we only extract spectra from a circle around the optical axis with radius 3.2', compared to 5' in HM06. Because of this and the excluded sources, the solid angle we use here is as small as 1/3 of that in HM06.

For each of the datasets, we fit the spectrum of the remaining area with a model consisting of an optically-thin thermal (APEC) component with solar abundances and  $kT \simeq 0.15$ – $0.2$  keV, to account for emission from the Galaxy as well as any diffuse thermal CXB. We also include a power law component that dominates at  $E > 1$  keV. We fix the power law photon index at  $\Gamma = 1.5$ , the best-fit value from HM06 (we do not vary  $\Gamma$  as in HM06, due to poorer statistics). A CDF-N VF spectrum with the model fit is shown in Fig. 2. We note that these models do not necessarily provide a physical description of the emission, but they are sufficient for our purpose of calculating fluxes.

For each spectrum, we calculate fluxes in six bands: 0.5–2 keV, 1–2 keV, 2–8 keV, and 2–5 keV, as well as the 0.65–1 keV and 1–1.3 keV bands, where the hypothetical WHIM signal or galaxy group emission are best distinguished from the diffuse Galactic foreground (see § 6). Errors on the observed flux include statistical errors in the sky and background count rates, and a 2% systematic uncertainty in the background normalization (§ 4 of HM06). We carefully account for background uncertainties; due to differences in pointing and large excluded areas (much larger than in HM06), the of the individual observations includes different stowed background photons. To account for this, we increase the effective exposure times of the composite background spectra by factors of  $\sim 3$  for CDF-N and  $\sim 1.5$  for CDF-S.

A further small correction is necessary to subtract the point source flux that is scattered outside our exclusion regions. For each *HST* or IRAC source, 10% of the X-ray flux should lie outside an exclusion region of radius  $r_{90}$ . However, because some regions overlap, the contribution of this scattered flux is smaller. Using a model of the *Chandra* PSF, we estimate that when all *HST* and IRAC

<sup>1</sup> [http://archive.stsci.edu/pub/hlsp/goods/catalog\\_r1/μr1.1z.readme.html](http://archive.stsci.edu/pub/hlsp/goods/catalog_r1/μr1.1z.readme.html)

<sup>2</sup> [http://data.spitzer.caltech.edu/popular/goods/Documents/goods\\_dataproducts.html](http://data.spitzer.caltech.edu/popular/goods/Documents/goods_dataproducts.html)

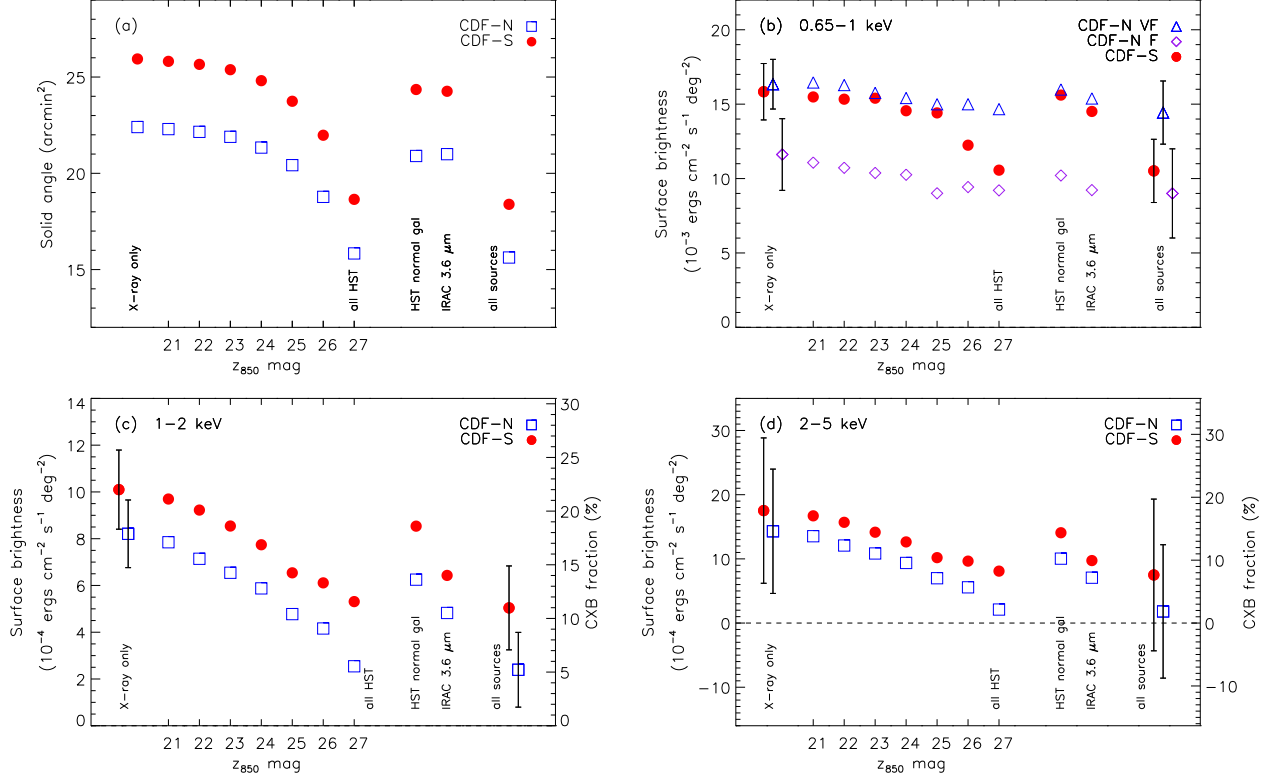


FIG. 3.— (a) Solid angles, and (b–d) unresolved CXB surface brightness, for subsets of excluded *HST* and IRAC sources. Values on the  $x$ -axis show maximum magnitudes for *HST*  $z_{850}$  sources. Note that  $z_{850} = 27$  is only an approximate detection limit for “all *HST*”. Points on the far left show the CXB signal when only X-ray sources are excluded (as in HM06), and points on the right show intensities excluding *HST* “normal” galaxies (§ 5.1), IRAC  $3.6 \mu\text{m}$  sources, and all *HST* and IRAC sources. For the 0.65–1 keV band we show the CDF-N VF and CDF-N F subsets separately, as time variability in the local emission (apparently charge exchange in the Solar wind, see Markevitch et al. 2003) caused these intensities to differ. For clarity, errors are shown only on the far left and right points. For (c) and (d), we show the fraction of the total CXB, for a power law CXB spectrum with  $\Gamma = 1.4$  and normalization  $10.9 \text{ photons cm}^{-2} \text{ s}^{-1} \text{ sr}^{-1}$  at 1 keV (HM06).

TABLE 1  
CXB SURFACE BRIGHTNESS AFTER EXCLUDING ALL SOURCES

Energy (keV)	CDF-S	CDF-N (VF+F)	Average	CXB frac. <sup>a</sup> (%)
0.5–2	$45 \pm 8$	$37 \pm 7^b$	$40 \pm 6^b$	...
0.65–1	$11 \pm 2$	$12 \pm 2^b$	$12 \pm 2^b$	...
1–2	$5.0 \pm 1.8$	$2.4 \pm 1.6$	$3.4 \pm 1.4$	$7.3 \pm 3.0$
1–1.3	$1.7 \pm 0.7$	$1.0 \pm 0.7$	$1.3 \pm 0.6$	$8.3 \pm 3.8$
2–5	$7 \pm 12$	$2 \pm 10$	$4 \pm 9$	$4 \pm 9$
2–8	$14 \pm 39$	$4 \pm 30$	$7 \pm 26$	$4 \pm 16$

NOTE. — Units are  $10^{-13} \text{ ergs cm}^{-2} \text{ s}^{-1} \text{ deg}^{-2}$ , errors are 68% confidence.

<sup>a</sup> Percent of total CXB, assuming a power-law CXB spectrum with  $\Gamma = 1.4$  and normalization  $10.9 \text{ photons cm}^{-2} \text{ s}^{-1} \text{ sr}^{-1} \text{ keV}^{-1}$  at 1 keV (HM06).

<sup>b</sup> Intensities for  $E < 1 \text{ keV}$  are dominated by Galactic and local line emission that varies with time and position. These are not extragalactic values.

<sup>c</sup> Only CDF-N F, to exclude the local temporary excess.

sources are excluded with radius  $r_{90}$ , 5% (0.5–2 keV) and 8% (2–8 keV) of their flux should remain in our unresolved spectrum. Likewise, 0.3% (0.5–2 keV) and 0.6% (2–8 keV) of the flux from the Alexander et al. (2003) X-ray point sources (for which we use larger exclusion regions) will be scattered into the spectrum. We account for both these small contributions in the final unresolved intensities. For a check, we also tried exclusion regions

of radius  $1.5r_{90}$ , and obtained identical results.

#### 4. RESULTS

We first calculate the CXB intensity after excluding the *HST* sources, using subsamples with various limiting magnitudes from  $z_{850} < 21$ –26, and finally excluding all *HST* sources ( $z \lesssim 27$ ). We also exclude only “normal” galaxies, selected based on their *HST* colors (see § 5.1), only the IRAC  $3.6 \mu\text{m}$  sources, and finally all *HST* and IRAC sources. The results are shown in Fig. 3. The residual CXB intensities excluding all sources (and an average for the three subsets) are given in Table 1. The calculation of these mean values includes a detailed error analysis, described in § 8.2.3 of HM06.

Fig. 3 shows excluding faint sources has little effect on the CXB at  $E < 1 \text{ keV}$ , where it is dominated by the truly diffuse Galactic and local emission. At  $E > 1 \text{ keV}$ , as fainter objects are excluded the surface brightness of the CXB decreases, indicating that the *HST* sources do indeed contribute to the X-ray unresolved CXB. In the 1–2 keV band, the remaining intensity after excluding all *HST* and IRAC sources is above zero at only  $1.5\sigma$  for CDF-N and  $2.8\sigma$  for CDF-S. The CXB intensity continues to decrease even to the faintest *HST* fluxes, suggesting that if we were able to exclude slightly fainter *HST*

sources, we would resolve the 1–2 keV CXB to within our absolute uncertainties. The X-ray undetected *HST* sources contribute 1–2 keV intensities of  $5.7 \times 10^{-13}$  and  $4.8 \times 10^{-13}$  ergs cm $^{-2}$  s $^{-1}$  deg $^{-2}$  in CDF-N and CDF-S, respectively, or 60% and 44% of the unresolved CXB signal found by HM06. These fluxes are significantly smaller than those of Worsley et al. (2006), who by stacking the X-ray flux from the same *HST* sources, find contributions of  $(8.4 \pm 0.5) \times 10^{-13}$  and  $(9.3 \pm 0.7) \times 10^{-13}$  ergs cm $^{-2}$  s $^{-1}$  deg $^{-2}$  for CDF-N and CDF-S, respectively.

In the 2–5 keV band, the *HST* and IRAC sources can account for the entire unresolved CXB within the large absolute uncertainties. This is similar to the results of Worsley et al. (2006), who find that the flux from *HST* sources is consistent with completely resolving the 2–6 keV CXB.

## 5. DISCUSSION

### 5.1. Which sources resolve the CXB?

Bauer et al. (2004) and HM06 show that AGN likely contribute a relatively small fraction of the CXB intensity at X-ray fluxes below the CDF limit. Instead, starburst and normal galaxies should become the dominant population of X-ray sources at  $S_{0.5-2 \text{ keV}} \lesssim 10^{-17}$  ergs cm $^{-2}$  s $^{-1}$ . To determine what class of galaxies gives the largest contribution to the unresolved CXB, we use *HST* colors to approximately divide the  $z_{850}$  sources into two subsets by galaxy type. While we do not have optical classifications for the *HST* GOODS galaxies, such a classification exists for the *HST* Ultra Deep Field (UDF), which covers a small 12 arcmin $^2$  region roughly 3' from the CDF-S aimpoint with a flux limit of  $z_{850} \simeq 30$ . The UDF was observed in the same four ACS bands as the wider GOODS fields, and Coe et al. (2006) performed a detailed photometric redshift analysis of the UDF sources, which classified each galaxy with one of eight templates (elliptical, Sab, Sbc, Im, and four types of starburst).

In Fig. 4, we show  $B_{435} - V_{606}$  vs.  $i_{775} - z_{850}$  colors for Coe et al. (2006) sources with  $z_{850} < 27$ , corresponding to the flux limits of the larger GOODS fields. Normal (elliptical and spiral) galaxies occupy different regions in this diagram from starburst and Im galaxies. This approximate region criteria ( $i_{775} - z_{850} > 0.2$  and  $B_{435} - V_{606} > 0.9 - [i_{775} - z_{850}]$ ) is shown in Fig. 4. Of the 255 “normal” galaxies in the sample, 201 (73%) are in this region, while only 52 (21%) of the 253 galaxies in this region have starburst or Im classifications and would be mis-classified by this criterion. Applying these criteria to the GOODS *HST* catalog, we classify roughly 25% of the  $z_{850}$  sources as “normal” galaxies. Fig. 3 shows that in the 1–2 keV band, the color-selected “normal” galaxies contribute  $\simeq 34\%$  to the total intensity resolved by the *HST* sources, while sources with “starburst/Im” colors account for  $\simeq 66\%$ .

We also examine the contribution from IRAC sources. Although the  $3.6 \mu\text{m}$  sources are on average only 0.25 magnitudes brighter in  $z_{850}$  than the *HST* sources, they account for a disproportionately large fraction of the unresolved CXB. The roughly 1000 IRAC sources contribute  $\simeq 63\%$  of the total 1–2 keV intensity resolved by all *HST* and IRAC sources. In comparison, the 1000 brightest *HST* sources (with  $z_{850} < 24.5$ ) account for

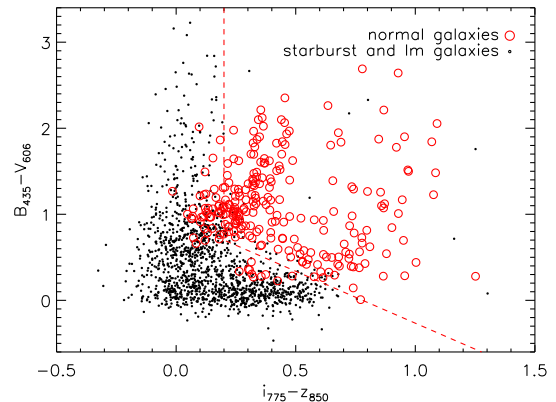


FIG. 4.— Color selection of “normal” galaxies from *HST* data. All points show  $B_{435} - V_{606}$  vs.  $i_{775} - z_{850}$  colors for sources in the UDF with  $z_{850} < 27$ . Sources are classified as elliptical and spiral galaxies (red circles) or starburst and Im galaxies (black dots) from photo- $z$  analysis (Coe et al. 2006). Lines show our criteria to select “normal” galaxies from the GOODS data.

$\simeq 53\%$ . Therefore, the X-ray flux from these objects is apparently more highly correlated with  $3.6 \mu\text{m}$  flux than  $z_{850}$  flux. This is likely an important clue as to the nature of these faint X-ray sources, although a detailed discussion is beyond the scope of this Letter. In a forthcoming paper, we will determine how bright the *HST* sources can be in the X-ray and whether *Chandra* could detect them in a reasonable longer exposure.

## 6. COMPARISON TO WHIM PREDICTIONS

While most of the remaining CXB signal should be due to Galactic or local diffuse emission and unresolved X-ray point sources, our results provide conservative upper limits on emission from the WHIM (Cen et al. 2000 and later works). The brightest WHIM emission feature should be a redshifted O VII 0.57 keV line. It cannot be distinguished from the bright Galactic O VII line without much better ( $\sim 1$  eV) spectral resolution, however the hotter WHIM phases with  $kT \sim 0.2 - 0.5$  keV would emit significant Fe XVII lines at  $E \approx 0.72 - 0.83$  keV. Thus, the ratio of WHIM emission to Galactic foreground (which is well-approximated by a  $kT \approx 0.15 - 0.2$  keV thermal spectrum, Fig. 1) may be higher at  $E \gtrsim 0.6$  keV.

We can compare our 0.65–1 keV signal with predictions from the cosmological simulations by Fang et al. (2005). Their WHIM intensities toward a galaxy group, filament, and void are  $\sim 3 \times 10^{-8}$ ,  $3 \times 10^{-10}$ , and  $3 \times 10^{-14}$  ergs cm $^{-2}$  s $^{-1}$  deg $^{-2}$ , respectively (where we approximately converted their 0.1–1 keV fluxes into 0.65–1 keV). Some recent simulations (Cen & Ostriker 2006) show that galactic superwinds may increase the WHIM metallicity, so the line emission may be even higher. The CDFs were selected to lie away from bright groups, but if they do not lie in voids, then our observed signal,  $1.2 \times 10^{-12}$  ergs cm $^{-2}$  s $^{-1}$  deg $^{-2}$ , comes interestingly close to the above predictions. At higher energies, our 1–2 keV signal is 15 times higher than the predicted sky-averaged WHIM intensity of  $0.19 \times 10^{-13}$  ergs cm $^{-2}$  s $^{-1}$  deg $^{-2}$  (Phillips et al. 2001). To perform a quantitative comparison to our measurements, it will be necessary to excise groups and regions around galaxies in the WHIM

simulations in a way similar to our analysis. With such a simulation, we may be able to place interesting constraints on the the distribution and metallicity of WHIM gas in the direction of the CDFs.

We thank J.P. Ostriker and L.A. Phillips for fruitful

discussions. RCH was supported by a NASA GSRP Fellowship NNG05GO20H and a Harvard Merit Fellowship, and MM by NASA contract NAS8-39073 and *Chandra* grant G04-5152X.

## REFERENCES

- Abazajian, K. N., et al. 2007, submitted to Phys. Rev. D, astro-ph/0611144  
 Alexander, D. M., et al. 2003, AJ, 126, 539  
 Bauer, F. E., et al. 2004, AJ, 128, 2048  
 Bertin, E. & Arnouts, S. 1996, A&AS, 117, 393  
 Cen, R. & Ostriker, J. P. 1999, ApJ, 514, 1  
 —. 2006, ApJ, 650, 560  
 Coe, D., et al. 2006, AJ, 132, 926  
 Davé, R., et al. 2001, ApJ, 552, 473  
 Dickinson, M., et al. 2003, in The Mass of Galaxies at Low and High Redshift, ed. R. Bender & A. Renzini, 324  
 Fang, T., et al. 2005, ApJ, 623, 612  
 Giavalisco, M., et al. 2004, ApJ, 600, L93  
 Hasinger, G., Miyaji, T., & Schmidt, M. 2005, A&A, 441, 417  
 Hickox, R. C. & Markevitch, M. 2006, ApJ, 645, 95  
 Kaastra, J. S., et al. 2006, ApJ, 652, 189  
 Markevitch, M., et al. 2003, ApJ, 583, 70  
 Moretti, A., et al. 2003, ApJ, 588, 696  
 Nicastro, F., et al. 2005, Nature, 433, 495  
 Phillips, L. A., Ostriker, J. P., & Cen, R. 2001, ApJ, 554, L9  
 Richards, E. A. 2000, ApJ, 533, 611  
 Ursino, E. & Galeazzi, M. 2006, ApJ, 652, 1085  
 Worsley, M. A., et al. 2006, MNRAS, 368, 1735  
 Worsley, M. A., et al. 2005, MNRAS, 357, 1281